European Polymer Journal 112 (2019) 531–538

Contents lists available at ScienceDirect

European Polymer Journal

journal homepage: www.elsevier.com/locate/europolj

Effect of synthetic colloidal nanoparticles in acrylic resin of dental use

Francisco Nunes de Souza Neto[a], Renata Lang Sala[a], Renan Aparecido Fernandes[b], Tatielih Pardim Oliveira Xavier[c], Sandra Andrea Cruz[a], Caio Marcio Paranhos[a], Douglas Roberto Monteiro[b,d], Debora Barros Barbosa[b], Alberto Carlos Botazzo Delbem[b], Emerson Rodrigues de Camargo[a,*]

[a] Federal University of São Carlos (UFSCar), Department of Chemistry, Interdisciplinary Laboratory of Electrochemistry and Ceramics (LIEC), Rod. Washington Luis, Km 235, São Carlos, SP 13565-905, Brazil
[b] State University of São Paulo (UNESP), Araçatuba Dental School, Department of Pediatric Dentistry and Public Health, Rua José Bonifácio 1193, Araçatuba, SP 16015-050, Brazil
[c] Federal Institute of Education Science and Technology of Goias – Campus Uruaçu (IFG), Rua Formosa, Qd 28 e 29, Loteamento Santana, Uruaçu, GO 76400-000, Brazil
[d] Graduate Program in Dentistry (GPD) – Master's Degree, University of Western São Paulo (UNOESTE), Rua José Bongiovani 700, Presidente Prudente, SP 19050-920, Brazil

ARTICLE INFO

Keywords:
Polymer-matrix composites
Silver nanoparticles
Structural composites
Thermo-mechanical properties
Antimicrobial properties

ABSTRACT

Acrylic resin employed in dental materials can act as substrate for microorganisms' adhesion and biofilm formation. To overcome this, silver nanoparticles (AgNPs) were combined with poly(methyl methacrylate) (PMMA) to reduce denture stomatitis caused by *Candida glabrata*. Although AgNPs antimicrobial activity is already known, the physicochemical properties of its nanocomposites, which dictate the performance of these commercial targets remain little explored. We evaluated the effect of different amount of AgNPs in PMMA obtained by the thermal polymerization. Among the mechanical tests employed, PMMA flexural strength decreased with higher AgNPs concentration. The microbiological adhesion test against *Candida glabrata* revealed the nanocomposite with 0.05% of AgNPs has greater capacity to inhibit the biofilm formed on its surface. Although we observed distinct thermo-mechanical behavior in the presence of AgNPs, antimicrobial property was not linearly dependent of nanoparticles concentration and was influenced by nanoparticles dispersion and distribution in the polymer matrix.

1. Introduction

Advances in material science during the last decades resulted in a new class of nanocomposite materials through the combination of polymeric matrices and a large number of different nanoparticles [1–7]. Considering their impact in the context of nanotechnology, metallic nanoparticles have physicochemical properties which differ from bulk materials [8–11].

In particular, AgNPs attracted considerable attention due to their numerous properties such as high thermal and electrical conductivity, surface enhanced Raman scattering, chemical stability and catalytic activity [12]. AgNPs have also demonstrated notorious antimicrobial activities against a large spectrum of viruses, fungi, and bacteria [13–16]. The antimicrobial efficiency of AgNPs is dependent on nanoparticles size [17], shape as triangular, rods and spherical, and synthesis methods [18,19]. The antimicrobial properties of nanocomposites filled with silver zeolite, citrate reduced silver nanoparticles, silver nitrate, metallic silver and laser ablated silver nanoparticles have been reported [19]. However, such antibacterial activity was not detected for the last two cases [13], demonstrating the degree of antimicrobial activity is greatly influenced by the type of silver particles [19] and their interaction with functional groups present in the membranes of microorganisms [20,21]. Silver nanoparticles can also inactivate important enzymes responsible by the replication of DNA in bacteria, which lead microorganisms to death [22,23].

The incorporation of silver nanoparticles (AgNPs) in a polymeric matrix increases the efficiency of antimicrobial action as well as reduces the transmission of infectious agents [24], being widely employed in food packaging combined with polymers as low density polyethylene films [13,25]. AgNPs were also incorporated in various biomaterials, with special attention to poly(methyl methacrylate) (PMMA) for medical and dental applications [26]. PMMA is a popular

* Corresponding author.
E-mail address: camargo@ufscar.br (E.R.d. Camargo).

https://doi.org/10.1016/j.eurpolymj.2018.10.009
Received 14 December 2017; Received in revised form 8 October 2018; Accepted 9 October 2018
Available online 13 October 2018
0014-3057/

biocompatible acrylic resin used in prosthesis fixation due to its chemical stability, commercial accessibility, and negligible toxicity [27,28]. However, colonization and biofilm formation of Candida on the surface of PMMA is the most common cause of denture stomatitis [29], a frequent oral lesion observed in prosthesis users [30]. With the incorporation of AgNPs in PMMA, nanocomposites can exhibit superior antimicrobial properties with effective control of common oral diseases in prosthesis users [31]. Meanwhile, the presence of AgNPs can also change mechanical properties and tensile strength of the final nanocomposite that could interfere in the materials performance [13,19].

In spite of the evident importance to develop simultaneously an acrylic resin with antimicrobial activity as well as safe, durable and comfortable materials for prosthesis users, the present work reported the synthesis of PMMA nanocomposites in the presence of AgNPs as potential material for dental use. Antifungal property against *Candida glabrata* (C. glabrata) microorganism was investigated through the incorporation of different concentrations of AgNPs, and correlated to the thermo-mechanical behavior, hardness and flexural strength of nanocomposites.

2. Experimental section

2.1. Synthesis of silver nanoparticles

Colloidal AgNPs were synthesized by an improved approach of Turkevich method that involves the reduction of silver nitrate ($AgNO_3$, 99%, Aldrich, USA) with the addition of sodium citrate ($Na_3C_6H_5O_7{\cdot}2H_2O$, 99%, Synth, Brazil) and ammonia (30%, analytical grade, Synth, Brazil) to control particle size. Initially, 1.0 mL of $AgNO_3$ aqueous solution (0.1 mol L^{-1}) and 1.0 mL of $Na_3C_6H_5O_7{\cdot}2H_2O$ aqueous solution (0.3 mol L^{-1}) were added to 100.0 mL of deionized water heated at 90 °C under stirring. The mixture was kept at this temperature until the appearance of a yellow color. Then, 1.0 mL of ammonia aqueous solution (1.4 mol L^{-1}) was added to finalize the synthesis [32].

2.2. Characterization of silver nanoparticles

The AgNPs synthesized were characterized by ultraviolet-visible (UV-Vis) spectrophotometry, X-ray diffraction (XRD), high-resolution transmission electronic microscopy (HRTEM) and dynamic light scattering (DLS). UV-Vis extinction spectra of AgNPs were obtained with a UV-Vis spectrophotometer (Jasco V-660) in the region of 300–800 nm, using a quartz cuvette. XRD analysis was performed in the Shimadzu XRD diffractometer with a Cu Kα radiation operating at 30 kV and 30 mA and 2θ range from 35 to 85° with step scan of 0.02° and scan speed of 0.2°·min^{-1}. To collect AgNPs patterns, nanoparticles were deposited on the surface of a silicon substrate (Si) by dripping the aqueous colloidal dispersion on the substrate at a room temperature, and the solvent was evaporated. The size and morphology of AgNPs synthesized were investigated by the HRTEM TECNAI F 20 Microscope operating at 80 kV. The samples were deposited on a carbon coated grid. DLS experiments were performed at room temperature and at a fixed angle of 173° on a Malvern Zetasizer Nano ZS equipped with 50 mW 533 nm laser and a digital auto correlator. In this method, the number-average values obtained were compared to the size distributions of the AgNPs.

2.3. Synthesis of PMMA and nanocomposites

The acrylic resin denture base Lucitone 550® was prepared according to the manufacturer's instructions. Each PMMA sample employed a ratio of 2.1 g powder (radical initiator – benzoyl peroxide) to 1.0 mL of liquid (monomer – PMMA) which were mixture and placed in metal molds (60 mm of length, 10 mm of width and 3 mm of thickness), and tightened with a hydraulic press with a load of 1 ton for 30 min [33]. The PMMA was polymerized in a warm water bath for 1.5 h at 73 °C followed by 30 min at 100 °C. After the thermal polymerization, the mold was cooled at room temperature and the polymer detached from the mold.

Aiming to obtain a material with potential application in dentistry, nanocomposites were prepared with coloration and texture similar to dental prosthesis. They were prepared in a similar synthetic route of PMMA. First, colloidal AgNPs were added in the monomer liquid component at the concentration of 0.05, 0.5 and 5% v/v, and subsequently slowly mixed with Lucitone 550® powder until the mixture reached the plastic form. Then, the nanocomposites were polymerized as described for pure PMMA and also reported by Monteiro et al. [31]. The final nanocomposites showed regular aspects and appearance, without visible heterogeneities from the presence of Ag nanoparticles.

2.4. Characterization of PMMA and nanocomposites

The PMMA and their nanocomposites were characterized by solid state nuclear magnetic resonance (ss-NMR), scanning electronic microscopy (SEM), thermogravimetric analysis (TGA), dynamic mechanical–thermal analysis (DMTA), hardness test and flexural strength.

The ss-NMR analyses were performed in a Bruker Avance III-400 equipped with a magic angle spinning (MAS) probehead. Samples were packed into a zirconia rotor. Spectra were obtained employing ^{13}C-CPTOSS (cross polarization with total sideband suppression), using adamantane as external reference. The contact time was of 3 ms, the recycle delay of 3 s, and spinning speed on magic angle of 5 kHz. The SEM images of PMMA and its nanocomposites were obtained at FEG-VP Zeiss Supra 35 with an accelerating voltage of 5 kV. To investigate the morphology of the fractured surfaces of samples, pellets were frozen using the liquid nitrogen and then fractured. After that, they were covered with a thin layer of gold. Polymer and nanocomposites degradation were evaluated by TGA using a NETZSCH TG 209F1 at a heating rate of 10 °C·min^{-1}, temperature range of 25–800 °C and nitrogen atmosphere. Mechanical properties were analyzed at DMTA 2980, TA Instruments Q800, in a frequency of 1 Hz. The temperature dependence of storage modulus (E′), loss modulus (E″) and loss tangent (tan δ) were evaluated from −100 to 160 °C at a heating rate of 2 °C·min^{-1}. The hardness was determined using a Micromet 5114 hardness tester (Buehler, Lake Bluff, USA) applying a 25 g load for 10 s. Each specimen was subjected to three penetrations observed on a monitor coupled to the microhardness tester. The three-point bending test was analyzed using a universal testing machine (DL 1000 EMIC) calibrated to provide a crosshead speed of 5 mm/min with a 500 kgf load cell.

2.5. Antimicrobial evaluation of PMMA and nanocomposites

2.5.1. Biofilm formation

Single biofilms of *C. glabrata* ATCC 90030 were formed on the surfaces of nanocomposites within 24-well microtiter plates (Costar, Tewksbury, EUA). An aliquot (1 mL) of the standardized cell suspension (1×10^7 cells mL^{-1} in artificial saliva – AS) was added to the wells. The plates were aerobically incubated at 37 °C during 48 h, with renewal of the AS medium after 24 h. After the biofilm formation period (48 h), the AS medium was aspirated, and each nanocomposite washed once with 1 mL of phosphate buffered saline (PBS, pH 7, 0.1 mol L^{-1}) to remove non-adherent cells. All assays were performed in triplicate, on three different occasions.

2.5.2. Quantification of total biofilm biomass

The total biomass was analyzed through the crystal violet (CV) staining method [34]. The resulting biofilms formed on the nanocomposites were fixed with 1 mL of 99% methanol (Sigma-Aldrich) within 24-well plates during 15 min. Subsequently, the nanocomposites were dried at room temperature and then 1 mL of CV stain (1%, v/v) (Sigma-Aldrich) was added into wells, and the plates incubated for

5 min. CV excesses were removed and the nanocomposites washed once with 1 mL of deionized water. Lastly, 1 mL of acetic acid (33%, v/v) (Sigma-Aldrich) was added into wells to solubilize the stain, and the obtained absorbance was read in a microtiter plate reader (Eon Microplate Spectrophotometer; Bio Tek, Winooski, USA) at 570 nm. All absorbance values were standardized in relation to the area of nanocomposites (Absorbance/cm^2).

2.5.3. Quantification of biofilm cultivable cells

Biofilms developed on the surface of nanocomposites were removed by sonication (30 W for 30 s) and vortexing (1 min), within falcon tubes containing 1 mL of PBS. Next, the biofilm suspensions were serially diluted in PBS and plated on CHROMagar Candida (Difco, Le Pont de Claix, France). After incubation at 37 °C for 24–48 h, the total number of colony-forming units (CFUs) per unit area (Log_{10} CFU/cm^2) of the nanocomposites was quantified.

2.5.4. Quantification of biofilm metabolic activity

The XTT (2,3-(2-methoxy-4-nitro-5-sulphophenyl)-5-[(phenylamino) carbonyl]-2H-tetrazolium hydroxide) (Sigma-Aldrich) reduction assay was applied to determine the metabolic activity of *C. glabrata* biofilms formed on the surface of nanocomposites [35]. After biofilm formation, the nanocomposites were washed once with PBS and transferred into new wells of 24-well plates containing 1 mL of a solution composed of 150 mg XTT/L and 10 mg phenazine methosulphate/L (Sigma-Aldrich). The plates were incubated for 3 h in the dark, at 37 °C under agitation (120 rpm). Absorbance values of the supernatant were measured at 490 nm and standardized per unit area of the nanocomposites (absorbance/cm^2). Wells containing nanocomposites inoculated with AS without *C. glabrata* were considered as blanks to measure the background levels.

2.5.5. Structural analysis of biofilms

SEM was performed to analyze the structure of *C. glabrata* biofilms. Single biofilms of *C. glabrata* ATCC 90030 were formed on the surface of nanocomposites, as described above. After biofilm formation (48 h), the nanocomposites were gently washed with PBS and then the biofilms were progressively dehydrated in ethanol (70% for 10 min, 95% for 10 min and 100% for 20 min). Finally, the nanocomposites were air dried, coated with gold and analyzed in an electron microscope (FEG-VP Zeiss Supra 35, Germany) operated at 5 kV.

2.5.6. Statistical analysis

SigmaPlot 12.0 software (Systat Software Inc., San Jose, USA) was employed for the statistical analysis with a confidence level of 95%. The test of Shapiro-Wilk was employed to determine the normality, the data passed on this test and then parametric statistical analyses were conducted using one-way ANOVA followed by post-hoc Holm-Sidak test.

3. Results and discussion

Single spherical AgNPs in water exhibit a typical intense plasmon resonance band around 420 nm in the extinction spectrum (Fig. 1a), which symmetrical shape of the plasmon band can indicate a relative sharp particle size distribution [36]. X-ray diffraction pattern (Fig. 1b) showed reflection patterns of face-centered cubic system (JCPDS file N° 04-0783). The reflection peak (2 2 4) belongs to the silicon substrate used as sample holder to collect the pattern. Domain of crystallographic coherence calculated by Scherrer equation reveled an average nanoparticles size of 7.2 nm.

Unlike other noble metals, only a fraction of Ag^+ ions reduces to form colloidal nanoparticles. Due to the presence of reminiscent ions in the medium, nuclei of AgNPs still keep forming while initially formed nanoparticles grow, resulting in a broader distribution of particle size. To solve this problem, ammonia in excess can be added to the system to form stable diamine silver complexes, resulting in AgNPs with controlled size [32]. HRTEM image of AgNPs (Fig. 1c) showed individual spherical AgNPs with sharp size distribution and average diameter of 7.6 nm ± 2.3 in Fig. 1d. Similarly, the AgNPs hydrodynamic diameter found by DLS analysis (Fig. 1e) was 5.8 nm ± 1.8, indicating AgNPs were formed and distributed as individual nanoparticles in aqueous dispersion with controlled size and distribution.

After the polymerization of PMMA in the presence of AgNPs (0.05, 0.5 and 5% v/v) to form nanocomposites, they were evaluated by structural, morphological, thermal and mechanical techniques as showed in Figs. 2–4, respectively.

Fig. 2 shows ^{13}C CP-TOSS NMR spectra of pure PMMA and their nanocomposites with different amounts of AgNPs. They showed five main peaks characteristic of PMMA without monomer residues, which respective carbon groups are illustrated on the top of Fig. 2. Chemicals shifts were assigned to carbonyl groups (C═O, 177.8 ppm), methylene groups (−CH_2−, 56.1 ppm), methoxy groups (−OCH_3, 51.9 ppm), polymer chain quaternary carbon (45.0 ppm) and methyl groups (−CH_3, 17.7 ppm) [37]. In the presence of AgNPs, nanocomposites showed similar spectra of pure PMMA, indicating they maintained the PMMA backbone structure.

Images of SEM (Fig. 3) from the fractured surfaces of samples reveled hollows filled with AgNPs on the surface of the PMMA nanocomposites. When larger volumes of AgNPs aqueous dispersion were added to monomers before the polymerization, greater amount of particles appeared distributed in the polymer matrix, forming some AgNPs agglomeration as shown in Fig. 3d. This effect can be a consequence of high surface tension during nanocomposites formation [38], especially considering the differences of surface tension between PMMA and the water (41×10^{-3} N·m^{-1} and 72×10^{-3} N·m^{-1}, respectively). Although some nanoparticles agglomeration was present, no visible heterogeneities were observed on nanocomposites surface.

Fig. 4 shows the thermal and mechanical behavior of PMMA and its nanocomposites, indicating the thermal degradation of the materials proceeds in three steps (Fig. 4a). The first step starts near to 200 °C and is characteristic of head-to-head linkages in PMMA structure of C═C bonds end groups, which are unstable [39]. The next two degradation steps are related to vinyl groups from terminal PMMA chains (−CH═CH_2), since their degradation occurs at lower temperatures (between 250 and 300 °C) than the saturated PMMA backbone, which degradation occurs between 300 and 400 °C [40,41]. This behavior is due to the lower stability of −CH═CH_2 groups, suffering a split in the β carbon.

To evaluate the thermal stability of nanocomposites, the initial mass loss temperature (T_{onset}) was determined by the intersection of the extrapolated starting mass with the tangent from the maximum slope of the TG curve. The maximum speed of mass loss temperature (T_{max}) was obtained by the peak of the first derivative and the difference between T_{max} and T_i (ΔT). Although the loss mass of samples occurs in three steps, T_{max} was calculated only for the third one, once this is the only process that has its temperature altered. The T_i was defined as the temperature where the third process initializes and presents the same value for all samples (305 °C). ΔT is an important parameter since it is possible to obtain information on the mass loss kinetics. The larger the ΔT value the slower is the release of volatiles during the degradation process [41]. Table 1 shows the parameters obtained from the TGA curves for the samples PMMA and PMMA-AgNPs.

The T_{onset} values (Table 1) increased for the PMMA-AgNPs when compared to pure PMMA, indicating the nanoparticles hindered the volatiles release at the initial step and could increase up to 40 °C the initial polymer degradation. Although T_{max} did not change for the second process, the intensity of the first derivative peak of percentage mass loss (Fig. 4a) was lower in function of higher nanoparticles content. The opposite behavior was observed for the third step, which means the presence of Ag promoted an increase in the mass loss. The increase in the area under the curve for the first derivative of mass loss confirms this statement. On the other hand, ΔT values (Table 1) showed

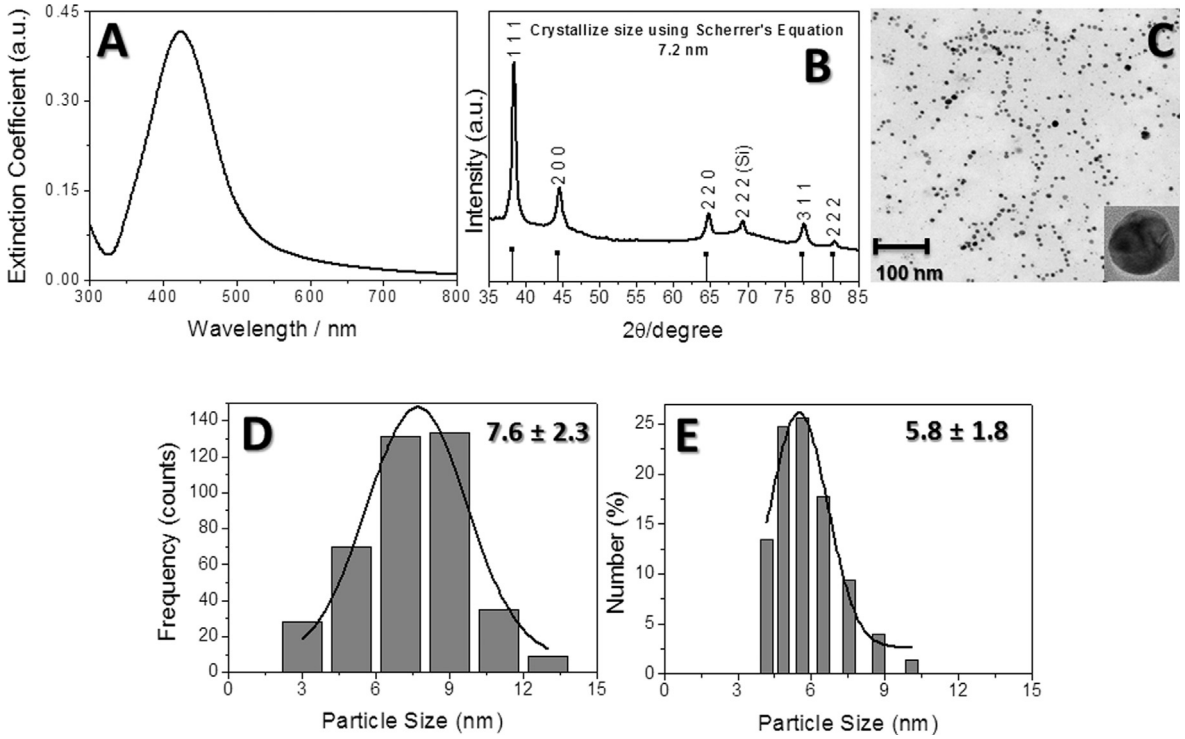

Fig. 1. (a) UV-Vis spectrum of AgNPs. (b) X-ray diffractographs of AgNPs. (c) TEM micrographs of AgNPs. (d) Size distributions by number of silver nanoparticles by DLS technique. (e) Histogram of TEM image of AgNPs.

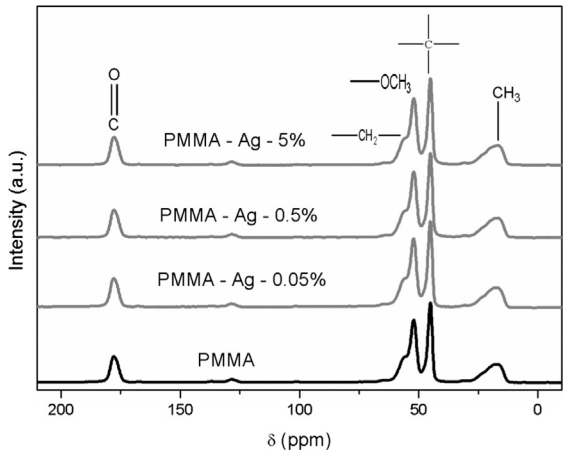

Fig. 2. ^{13}C CP-TOSS NMR spectra of PMMA and its nanocomposites.

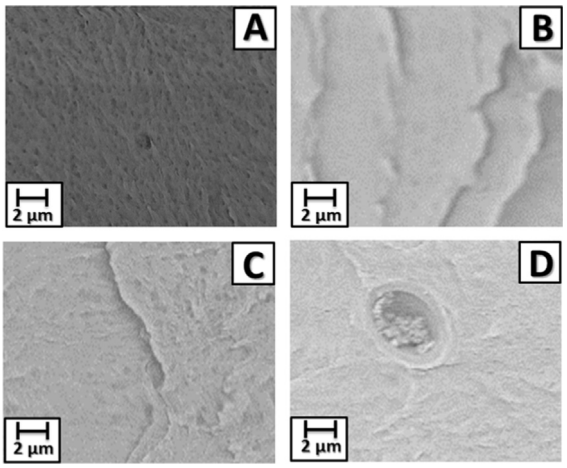

Fig. 3. SEM images of PMMA and its nanocomposites. (a) PMMA; (b) PMMA-Ag-0.05%; (c) PMMA-Ag-0.5% and (d) PMMA-Ag-5%.

the mass loss evolution is slower due to the presence of nanoparticles, indicating that although AgNPs promotes an increase in the mass loss, the nanocomposites degradation kinetics is slower. These results may be explained by different mechanisms. First, AgNPs presence causes a reduction in the effect of thermal inertia due to the difference of conductivity between both materials (k PMMA = 0.2 $W m^{-1} K^{-1}$; k Ag = 400 $W m^{-1} K^{-1}$), favoring the processes of mass loss at higher temperatures. Second, the higher the AgNPs content, the slower the gases diffusion through the polymeric mass. This barrier effect generated by the presence of AgNPs increases the mean free path of the gas in the polymeric bulk [41] decreasing the volatiles release kinetics and shifting T_{max} for higher temperatures. Studies reported by Vodnik et al. [42,43] also demonstrated that the incorporation of different AgNPs concentrations in PMMA increased the initial thermal stability of the nanocomposites and their thermal degradation shifted toward higher temperature.

DMTA technique was employed to study the materials capability to store and dissipate the mechanical energy by evaluating the storage modulus (E′), loss modulus (E″) (Fig. 4b) and tan δ (Fig. 4c). In Fig. 4b, the DMTA analysis showed a marked drop in the storage modulus (E′) between the region of −100 and 160 °C, considered the primary relaxation (α) for amorphous PMMA. It results from motions of polymer chain segments at long distances. PMMA samples also present the β-relaxation in that region related to the rotation of the methoxy-carbonyl side group linked to the main chain (local molecular motions), presented in the glassy state of polymer between -100 and 100 °C [17,44].

When nanoparticles were presented in the PMMA, E′, E″ and tan δ were almost the same for the nanocomposites with lower concentration of AgNPs in both glassy and rubbery states, excepting the PMMA-Ag-5% nanocomposite, which showed reduced modulus when compared to pure PMMA, especially in the glassy state. The reduction of this modulus combined to the slight reduced of T_g and β-relaxation, observed by

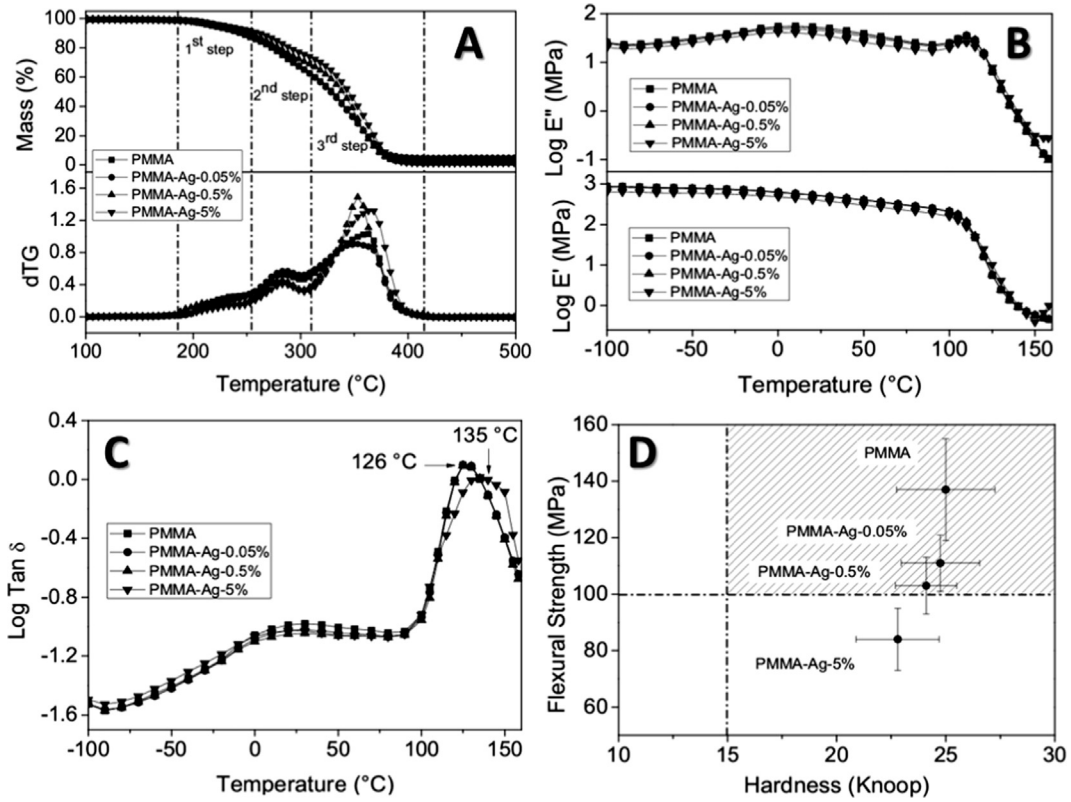

Fig. 4. Thermal and mechanical behavior of PMMA and its nanocomposites. (a) Thermogravimetric and first derivative of the percentage mass loss curves of PMMA and its nanocomposites. (b) Loss modulus (E″) and storage modulus (E') curves of PMMA and its nanocomposites. (c) Tan δ curves of PMMA and its nanocomposites. (d) Flexural strength and hardness of PMMA and its nanocomposites.

Table 1
Thermal parameters obtained from the TGA curves for PMMA and its nanocomposites with different AgNPs content.

Sample	T_{onset}	T_{max}	ΔT ($T_{max} - T_i$)*
PMMA	265	353	48
PMMA-Ag-0.05%	265	352	47
PMMA-Ag-0.5%	289	363	58
PMMA-Ag-5%	308	366	61

* T_i represents the temperature of initial mass loss for the third step (305 °C for all samples).

the peaks of tan δ curves at Fig. 4c, is assigned to a plasticizing effect, since the local and long distance chain motions were facilitated by the incorporation of nanoparticles distributed in the polymer matrix [45]. In this context, Pandis et al. [46] observed similar results when AgNPs were added in PMMA. They observed a decrease in E', E" and the glass transition temperature by increasing nanoparticles concentration. This behavior could be explained by a weak polymer-nanoparticles interaction and increase of free volume in the nanocomposites with loosed polymer chains packing near the nanoparticles, resulting in the same observed plasticizing effect. In this sense, depending on the concentration of silver nanoparticles, the final thermo-mechanical properties can be changed when compared to pure PMMA. Controlling these properties, applications as dental implants and their durability can be deeply understood.

Fig. 4d shows the correlation between the strength modulus and the hardness obtained for PMMA and its nanocomposites, where the dashed lines represent the minimum acceptable hardness and flexural strength of acrylic resins for intraoral prosthesis, 15.00 Knoop and 1000 Mpa, respectively [47,48]. These values are in agreement with the specification N° 12 of the American Dental Association 1958 reference and the ISO 4049 standard. The obtained values indicated a slight decrease of flexural strength according to AgNPs content and similar hardness for all materials. Although all materials could be clinically accepted by their hardness values, PMMA-Ag-5% had an value of flexural strength bellow the recommendation. Small differences in the mechanical behaviour of PMMA nanocomposites can be related to weak interactions between nanoparticles and acrylic chains as observed in DMTA analysis. Additionally, the degree of nanoparticles dispersion could also affect the flexural strength of nanocomposites [18,33], reducing it by the presence of nanoparticles agglomeration. Sodagar et al. [33] observed opposite behavior of the flexural strength from acrylate resins from different brands in the presence of AgNPs. For one resin, the presence of AgNPs increased the flexural strength and for the other resin, the presence of nanoparticles reduced it. These differences were associated to the chemical composition of the resin, amount of nanoparticles and polar interaction between AgNPs and C═O from PMMA [18].

It is a general accepted idea that every nanoparticle should improve mechanical properties of nanocomposites through attractive interactions. Nanocomposites are better evaluated when considering their final performance than in terms of interactions between nanoparticles and polymeric chains. Nanocomposites of AgNPs and PMMA are good examples of functional materials that can exhibit improved performance against microorganisms without any benefit in mechanical property. In fact, pure PMMA is widely used to fabricate dental prosthesis with excellent mechanical performance without the necessity of any mechanical gain due to the insertion of nanoparticles. Also, it is desired a balance between these properties, since flexural strength is useful in predicting the evaluation of fracture resistance, while hardness indicates the rigidity necessary to confer comfort to the patient during chewing. Therefore, the hatched area showed in Fig. 4d indicates that the nanocomposites PMMA-Ag-0.05% and PMMA-Ag-0.5% could be potential commercial targets.

The treatment of biofilm-mediated infections has become a challenge due to their drug resistance generated by the dense matrix formed by the microbial cells. One strategy is the AgNPs targeting antibiofilm therapy, which has gained attention due to nanoparticles antimicrobial properties and ability of reactive entities infiltrate into the biofilm matrix, which generally forms a barrier for many medicines [49].

Biofilm formation by *Candida* species, as *Candida albicans* and *Candida glabrata* is a common form of oral infection found in denture stomatitis [50]. Although *C. glabrata* is responsible for no more than 15% of mucosal and systemic candidiasis, it exhibits superior adhesion to acrylic surfaces than *C. albicans*. Then, *C. glabrata* is a suitable pathogenic to evaluate the adherence of biofilms on PMMA based nanocomposites [51]. Usually, mechanical cleansing provides enough cleanliness, except for geriatric or handicapped denture wearers whose manual dexterity may be compromised. These special cases require functional superfaces with reduced adhesion of microorganisms.

Once single biofilms of *C. glabrata* were cultured on the surfaces of nanocomposites after 48 h of incubation, the quantification of biofilm biomass was obtained with CV staining assay and the total number of CFUs, where CV staining assay does not differentiate between live and dead cells and is used as a complement to CFU [50]. In the CV assay, the increase of absorption intensities at 570 nm in Fig. 5a is proportionally to the total biofilm biomass. Using pure PMMA as control, nanocomposites effectively reduced the total biomass of *C. glabrata* in 35%, 17% and 28% ($P = 0.026$) for PMMA-Ag-0.05%, PMMA-Ag-0.5% and PMMA-Ag-5%, respectively. Additionally, the nanocomposite containing the lowest concentration and dispersed silver nanoparticles (0.05%) reduced the metabolic activity of *C. glabrata* biofilms (57% $P = 0.007$). Regarding the number of colony-forming units (CFUs) per area, there is no significant differences among observed groups (Fig. 5b).

Usually, there is a linear relationship between free AgNPs and biofilm inhibition [52], but at first glance, Fig. 5a indicated an independence of AgNPs amount and the total biomass produced by microorganisms. Actually, these values reveled the direct influence of AgNPs agglomerates against the formation of biofilms on the surface of PMMA than the action of individual silver nanoparticles. Measurements of metabolic activity of *C. glabrata* biofilms at 490 nm by XTT assays [53] confirmed the assumption that large amounts of AgNPs in PMMA nanocomposites form agglomerates instead of a homogeneous distribution of free nanoparticles (as showed in Fig. 3), and consequently large amounts of AgNPs are less effective against formation of biofilms.

Regardless of the extensive literature about antimicrobial activity of silver nanoparticles against microorganisms [54], it is suggested that the antimicrobial activity of AgNPs incorporated in polymers depends on the ion release. When AgNPs are in direct contact with the microorganisms, they may cause disruption of the vital functions of bacteria/fungi and the generation of reactive oxygen species. Moreover, the release of silver ions may interfere with DNA replication through chemical reactions with the thiol groups [53].

The release of silver ions can be related to the diffusion of water molecules inside the acrylic resin and migration of ions through the polymer to the aqueous medium. The acrylic resin Lucitone 550 contains a crosslinking agent (ethylene glycol dimethacrylate) responsible for increasing the rigidity of the polymeric structure. Accordingly, silver nanoparticles were trapped inside the polymer chains and their release into the aqueous medium could be restricted. Therefore, the absence of antifungal property observed for PMMA-Ag nanocomposites could be related to poor release of silver ions or silver nanoparticles from the samples [55]. Previous study demonstrated no release of Ag nanoparticles overtime when PMMA-AgNPs nanocomposites were incubated in deionized water at 37 °C [31]. Although this study was conducted during 120 days, it demonstrated undetectable amount of released nanoparticles. In this way, while the release of silver nanoparticles can improve the antimicrobial activity of some materials, the presence of AgNPs trapped inside the resin will retain the performance of nanocomposites overtime and enable their potential application for dental use.

Fig. 6 shows biofilms of *C. glabrata* attached on the surface of pure PMMA and its nanocomposites, constituted by multilayer yeast completely covering the surface. The acrylic resin showed a microorganism cluster with spherical shape adhered on its surface. Moreover, nanocomposites did not show a significant reduction of *C. glabrata* adhesion on its surface as demonstrated by the CFU test in Fig. 5b, as well as no structural modifications of *C. glabrata* cells in Fig. 6. However, biofilms formed on the surfaces of the PMMA-Ag-0.05% and PMMA-Ag-0.5% nanocomposites exhibited less compact structures with cells partially covering surfaces, particularly the PMMA-Ag-0.05%. Hamid et al. [56] also observed an irregular and reduced adherence of *C. albicans* and *C. parapsilosis* biofilm on urinary catheter treated with mycogenic AgNPs, however they did not investigate how the concentration of AgNPs coated catheter affects the biofilm attachment.

4. Conclusions

The addition of AgNPs in nanocomposites can lead to higher initial mass loss temperature and slower volatiles release kinetics in TGA. Depending on the AgNPs concentration, they can generate a plasticizing effect in PMMA matrix and reduce its mechanical properties as showed by DMTA and flexural strength. Silver nanoparticles were agglomerated in the nanocomposite with 5% of AgNPs, which also demonstrated reduced flexural strength and less efficient *C. glabrata* biofilm inhibition. Among the nanocomposites, the PMMA with 0.05% of AgNPs showed the most promising properties for medical and dental applications, since it showed adequate mechanical performance for dental prosthesis, effectively reduced the metabolic activity of *C. glabrata* biofilms as well

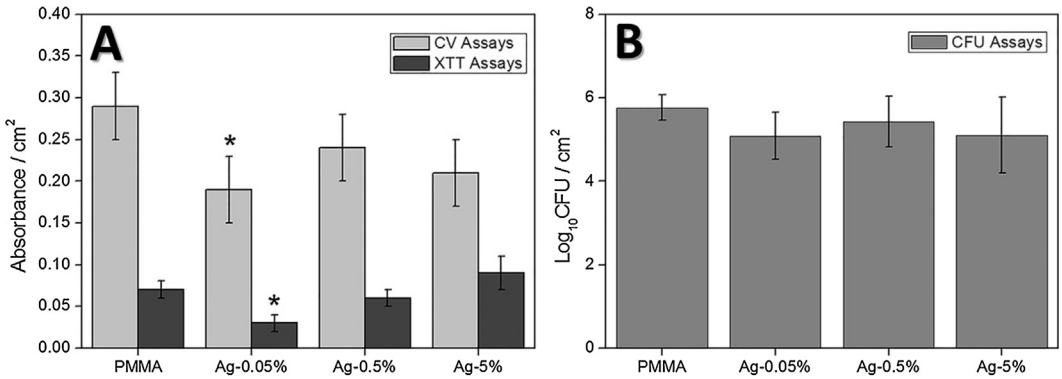

Fig. 5. (a) Average absorbance at 570 and 490 nm per cm^2 obtained for PMMA and its nanocomposites in crystal violet (CV) assay and XTT reduction assay for *C. glabrata*, respectively. (b) Mean values of the logarithm of colony forming units per cm^2 (log_{10} CFU/cm^2) for *C. glabrata* for PMMA and its nanocomposites.

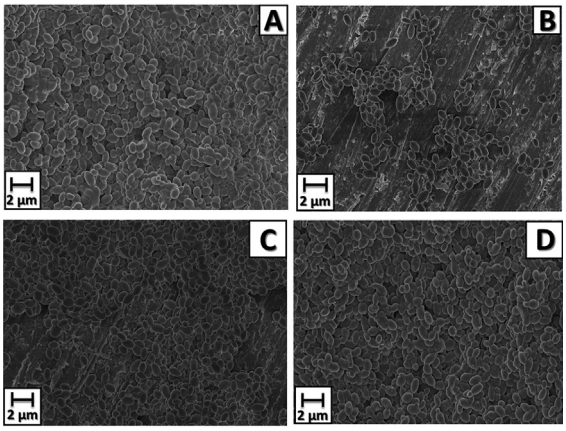

Fig. 6. Micrographs of *C. glabrata* biofilms developed on the surface of (a) pure PMMA as control group, (b) PMMA-Ag-0.05%, (c) PMMA-Ag-0.5% and (d) PMMA-Ag-5%.

as the biofilm inhibition and adhesion.

Acknowledgements

Authors acknowledge the Brazilian agencies São Paulo Research Foundation (FAPESP) (grants 2012/07067-0, 2012/17880-0, 2015/13958-3) for financial support and for the concession of a scholarship, National Council for Scientific and Technological Development (CNPq) and Coordination of Higher Education Personnel (CAPES) for financial support. The authors declare no potential conflicts of interest with respect to the authorship and/or publication of this article.

References

[1] P. Dallas, V.K. Sharma, R. Zboril, Silver polymeric nanocomposites as advanced antimicrobial agents: classification, synthetic paths, applications, and perspectives, Adv. Colloid Interface Sci. 166 (2011) 119–135.
[2] S. Komarneni, Nanocomposites, J. Mater. Chem. 2 (12) (1992) 1219–1230.
[3] R.M. Laine, J. Choi, I. Lee, Organic-inorganic nanocomposites with completely defined interfacial interactions, Adv. Mater. 13 (11) (2001) 800–803.
[4] F. Hussain, M. Hojjati, M. Okamoto, R.E. Gorga, Review article: polymer-matrix nanocomposites, processing, manufacturing, and application: an overview, J. Compos. Mater. 40 (17) (2006) 1511–1575.
[5] S. Kango, S. Kalia, A. Celli, J. Njuguna, Y. Habibi, R. Kumar, Surface modification of inorganic nanoparticles for development of organic–inorganic nanocomposites—a review, Prog. Polym. Sci. 38 (2013) 1232–1261.
[6] T.M. Arantes, R.L. Sala, E.R. Leite, E. Longo, E.R. Camargo, Comparison of the nanoparticles performance in the photocatalytic degradation of a styrene–butadiene rubber nanocomposite, J. Appl. Polym. Sci. 128 (4) (2013) 2368–2374.
[7] D. Miracle, Metal matrix composites – from science to technological significance, Comp. Sci. Technol. 65 (15–16) (2005) 2526–2540.
[8] J. Dai, M.L. Bruening, Catalytic nanoparticles formed by reduction of metal ions in multilayered polyelectrolyte films, Nano Lett. 2 (5) (2002) 497–501.
[9] N.D. Luong, Y. Lee, J.D. Nam, Highly-loaded silver nanoparticles in ultrafine cellulose acetate nanofibrillar aerogel, Eur. Polym. J. 44 (2008) 3116–3121.
[10] A.M. Kubo, L.F. Gorup, L.S. Amaral, E.R. Filho, E.R. Camargo, Kinetic control of microtubule morphology obtained by assembling gold nanoparticles on living fungal biotemplates, Bioconjugate Chem. 27 (10) (2016) 2337–2345.
[11] O. Peña-Rodriguez, A. Prada, J. Olivares, A. Oliver, L. Rodriguez-Fernandez, H.G. Silva-Pereyra, E. Bringa, J.M. Perlado, A. Rivera, Understanding the ion-induced elongation of silver nanoparticles embedded in silica, Sci. Rep. 7 (2017) 922–930.
[12] A. Haider, I.K. Kang, Preparation of silver nanoparticles and their industrial and biomedical applications: a comprehensive review, Adv. Mater. Sci. Eng. 2015 (2015) 1–16.
[13] S. Kumar, M. Sarita, N. Nehra, K. Dilbaghi, K.-H. Tankeshwar, Kim, Recent advances and remaining challenges for polymeric nanocomposites in healthcare applications, Prog. Polym. Sci. 80 (2018) 1–38.
[14] A.K. Suresh, D.A. Pelletier, M.J. Doktycz, Relating nanomaterial properties and microbial toxicity, Nanoscale 5 (2013) 463–474.
[15] L. Dai, B. Nadeau, X. An, D. Cheng, Z. Long, Y. Ni, Silver nanoparticles-containing dual-function hydrogels based on a guar gum-sodium borohydride system, Sci. Rep. 6 (2016) 36497–36502.
[16] C. You, Q. Li, X. Wang, P. Wu, J.K. Ho, R. Jin, L. Zhang, H. Shao, C. Han, Silver nanoparticle loaded collagen/chitosan scaffolds promote wound healing via regulating fibroblast migration and macrophage activation, Sci. Rep. 7 (2017) 10489–10499.
[17] P. Oyar, F.A. Sana, R. Durkan, Comparison of mechanical properties of heat-polymerized acrylic resin with silver nanoparticles added at different concentrations and sizes, J. Appl. Polym. Sci. 135 (2018) 45807–45812.
[18] A. Koroglu, O. Sahin, I. Kurkcuoglu, D.O. Dede, T. Ozdemir, B. Hazer, Silver nanoparticle incorporation effect on mechanical and thermal properties of denture base acrylic resins, J. Appl. Oral Sci. 24 (6) (2016) 590–596.
[19] S. Shankar, L.F. Wang, J.W. Rhim, Preparations and characterization of alginate/silver composite films: effect of types of silver particles, Carbohyd. Polym. 146 (2016) 208–216.
[20] R. Kumar, H. Munstedt, Silver ion release from antimicrobial polyamide/silver composites, Biomaterials 26 (2005) 2081–2088.
[21] C. Damm, H. Münstedt, A. Rösch, The antimicrobial efficacy of polyamide 6/silver-nano- and microcomposites, Mater. Chem. Phys. 108 (2008) 61–66.
[22] C. Fan, L. Chu, H.R. Rawls, B.K. Norling, H.L. Cardenas, K. Whang, Development of an antimicrobial resin–a pilot study, Dent. Mater. 27 (2011) 322–328.
[23] T.C. Dakal, A. Kumar, R.S. Majumdar, V. Yadav, Mechanistic basis of antimicrobial actions of silver nanoparticles, Front. Microbiol. 7 (2016) 1831–1847.
[24] H. Kong, J. Jang, Antibacterial properties of novel Poly(methyl methacrylate) nanofiber containing silver nanoparticles, Langmuir 24 (2008) 2051–2056.
[25] S. Azlin-Hasim, M.C. Cruz-Romero, M.A. Morris, E. Cummins, J.P. Kerry, Effects of a combination of antimicrobial silver low density polyethylene nanocomposite films and modified atmosphere packaging on the shelf life of chicken breast fillets, Food Packag. Shelf Life 4 (2015) 26–35.
[26] Y.H. Hsueh, K.S. Lin, W.J. Ke, C.T. Hsieh, C.L. Chiang, D.Y. Tzou, S.T. Liu, The antimicrobial properties of silver nanoparticles in bacillus subtilis are mediated by released Ag^+ ions, PloS One 10 (2015) 1–17.
[27] A. Sodagar, B. Azizy, M.Z. Kassaee, B. Pourakbari, S. Arab, A. Bahador, Anti-cariogenic effect of polymethylmethacrylate with in situ generated silver nanoparticles on planktonic and biofilm bacteria, Ann. Biol. Res. 4 (8) (2013) 211–219.
[28] A. Bahador, B. Pourakbari, R. Ghorbanzadeh, S.O. Moghadam, A. Sodagar, Antibacterial effects of polymethylmethacrylate with in situ generated silver nanoparticles on primary colonizers of human dental plaque and cariogenic bacteria, Annu. Res. Rev. Biol. 4 (10) (2014) 1587–1601.
[29] E. Uzunoglu, A.Z. Yildirim Bicer, I. Dolapci, A. Dogan, Biofilm-forming ability and adherence to poly-(methyl-methacrylate) acrylic resin materials of oral Candida albicans strains isolated from HIV positive subjects, J. Adv. Prosthodont. 6 (2014) 30–34.
[30] J. Wen, F. Jiang, C.K. Yeh, Y. Sun, Controlling fungal biofilms with functional drug delivery denture biomaterials, Colloids Surf. B. 140 (2016) 19–27.
[31] D.R. Monteiro, L.F. Gorup, A.S. Takamiya, E.R. Camargo, A.C. Ruvolo Filho, D.B. Barbosa, Silver distribution and release from an antimicrobial denture base resin containing silver colloidal nanoparticles, J. Prosthodont. 21 (2012) 7–15.
[32] L.F. Gorup, E. Longo, E.R. Leite, E.R. Camargo, Moderating effect of ammonia on particle growth and stability of quasi-monodisperse silver nanoparticles synthesized by the Turkevich method, J. Colloid. Interf. Sci. 360 (2011) 355–358.
[33] A. Sodagar, M.Z. Kassaee, A. Akhavan, N. Javadi, S. Arab, M.J. Kharazifard, Effect of silver nano particles on flexural strength of acrylic resins, J. Prosthodont. Res. 56 (2012) 120–124.
[34] D.R. Monteiro, L.F. Gorup, S. Silva, M. Negri, E.R. de Camargo, R. Oliveira, D.B. Barbosa, M. Henriques, Silver colloidal nanoparticles: antifungal effect against adhered cells and biofilms of *Candida albicans* and *Candida glabrata*, Biofouling 27 (7) (2011) 711–719.
[35] S. Hawser, Comparisons of the susceptibilities of planktonic and adherent *Candida albicans* to antifungal agents: a modified XTT tetrazolium assay using synchronised *C. albicans* cells, J. Med. Vet. Mycol. 34 (2) (1996) 149–152.
[36] S. Pal, Y.K. Tak, J.M. Song, Does the antibacterial activity of silver nanoparticles depend on the shape of the nanoparticle? A study of the Gram-negative bacterium *Escherichia coli*, Appl. Environ. Microb. 73 (2007) 1712–1720.
[37] R. Avolio, G. Gentile, M. Avella, D. Capitani, M.E. Errico, Synthesis and characterization of poly(methylmethacrylate)/silica nanocomposites: study of the interphase by solid-state NMR and structure/properties relationships, J. Polym. Sci. A1 48 (23) (2010) 5618–5629.
[38] R. Qiao, H. Deng, K.W. Putz, L.C. Brinson, Effect of particle agglomeration and interphase on the glass transition temperature of polymer nanocomposites, J. Polym. Sci. Pol. Phys. 49 (2011) 740–748.
[39] M. Ferriol, A. Gentilhomme, M. Cochez, N. Oget, J.L. Mieloszynski, Thermal degradation of poly(methyl methacrylate) (PMMA): modelling of DTG and TG curves, Polym. Degrad. Stabil. 79 (2003) 271–281.
[40] P.H.F. Oliveira, S.T. Amancio-Filho, J.F. dos Santos, E. Hage, Preliminary study on the feasibility of friction spot welding in PMMA, Mater. Lett. 64 (2010) 2098–2101.
[41] L.B. Fitaroni, J.A. de Lima, S.A. Cruz, W.R. Waldman, Thermal stability of polypropylene–montmorillonite clay nanocomposites: limitation of the thermogravimetric analysis, Polym. Degrad. Stabil. 111 (2015) 102–108.
[42] V.V. Vodnik, J.V. Vuković, J.M. Nedeljković, Synthesis and characterization of silver—poly(methylmethacrylate) nanocomposites, Colloid Polym. Sci. 287 (2009) 847–851.
[43] V.V. Vodnik, D.K. Božanić, E. Džunuzović, J. Vuković, J.M. Nedeljković, Thermal and optical properties of silver–poly(methylmethacrylate) nanocomposites prepared by in-situ radical polymerization, Eur. Polym. J. 46 (2010) 137–144.
[44] D. Ionita, M. Cristea, D. Banabic, Viscoelastic behavior of PMMA in relation to deformation mode, J. Therm. Anal. Calorim. 120 (2015) 1775–1783.
[45] E.T. Kopesky, T.S. Haddad, G.H. McKinley, R.E. Cohen, Miscibility and viscoelastic properties of acrylic polyhedral oligomeric silsesquioxane–poly(methyl methacrylate) blends, Polymer 46 (2005) 4743–4752.

[46] C. Pandis, E. Logakis, A. Kyritsis, P. Pissis, V.V. Vodnik, E. Džunuzović, J.M. Nedeljković, V. Djoković, J.C. Rodríguez Hernández, J.L. Gómez Ribelles, Glass transition and polymer dynamics in silver/poly(methyl methacrylate) nanocomposites, Eur. Polym. J. 47 (2011) 1514–1525.
[47] M.C. Goiato, D.M. Dos Santos, A.M. Andreotti, A.S. Nobrega, A. Moreno, M.F. Haddad, A.A. Pesqueira, Effect of beverages and mouthwashes on the hardness of polymers used in intraoral prostheses, J. Prosthodont. 23 (2014) 559–564.
[48] F. Liu, B. Sun, X. Jiang, S.S. Aldeyab, Q. Zhang, M. Zhu, Mechanical properties of dental resin/composite containing urchin-like hydroxyapatite, Dent. Mater. 30 (12) (2014) 1358–1368.
[49] S. Qayyum, A.U. Khan, Nanoparticles vs. biofilms: a battle against another paradigm of antibiotic resistance, MedChemComm 7 (2016) 1479–1498.
[50] D.R. Monteiro, A.S. Takamiya, L.P. Feresin, L.F. Gorup, E.R. de Camargo, A.C. Delbem, M. Henriques, D.B. Barbosa, Susceptibility of *Candida albicans* and *Candida glabrata* biofilms to silver nanoparticles in intermediate and mature development phases, J. Prosthodont. Res. 59 (2015) 42–48.
[51] K. Zomorodian, N.N. Haghighi, N. Rajaee, K. Pakshir, B. Tarazooie, M. Vojdani, F. Sedaghat, M. Vosoghi, Assessment of Candida species colonization and denture-related stomatitis in complete denture wearers, Med. Mycol. 49 (2011) 208–211.
[52] K. Kalishwaralal, S. BarathManiKanth, S.R. Pandian, V. Deepak, S. Gurunathan, Silver nanoparticles impede the biofilm formation by Pseudomonas aeruginosa and Staphylococcus epidermidis, Colloids Surf. B 79 (2010) 340–344.
[53] A.F. Wady, A.L. Machado, C.C. Foggi, C.A. Zamperini, V. Zucolotto, E.B. Moffa, C.E. Vergani, Effect of a silver nanoparticles solution on Staphylococcus aureus and Candida spp. J. Nanomater. 2014 (2014) 1–7.
[54] M.Z. Kassaee, A. Akhavan, N. Sheikh, A. Sodagar, Antibacterial effects of a new dental acrylic resin containing silver nanoparticles, J. Appl. Polym. Sci. 110 (3) (2008) 1699–1703.
[55] A.F. Wady, A.L. Machado, V. Zucolotto, C.A. Zamperini, E. Berni, C.E. Vergani, Evaluation of *Candida albicans* adhesion and biofilm formation on a denture base acrylic resin containing silver nanoparticles, J. Appl. Microbiol. 112 (2012) 1163–1172.
[56] S. Hamid, S. Zainab, R. Faryal, N. Ali, Deterrence in metabolic and biofilms forming activity of *Candida* species by mycogenic silver nanoparticles, J. Appl. Biomed. 15 (4) (2017) 249–255.